BMC Medical Imaging

RESEARCH

Open Access

Desmoplastic Small Round Cell Tumor: a study of CT, MRI, PET/CT multimodal imaging features and their correlations with pathology

Kaiwei Xu[1†], Yi Chen[2†], Wenqi Shen[1,3†], Fan Liu[4†], Ruoyu Wu[1], Jiajing Ni[1,3], Linwei Wang[1,3], Chunqu Chen[1], Lubin Zhu[1,3], Weijian Zhou[1,3], Jian Zhang[5*], Changjing Zuo[6*] and Jianhua Wang[4*]

Abstract

Purpose Exploring the computed tomography (CT), magnetic resonance imaging (MRI), and fluorodeoxyglucose positron emission tomography (FDG-PET)/CT Multimodal Imaging Characteristics of Desmoplastic Small Round Cell Tumor (DSRCT) to enhance the diagnostic proficiency of this condition.

Methods A retrospective analysis was performed on clinical data and multimodal imaging manifestations (CT, MRI, FDG-PET/CT) of eight cases of DSRCT. These findings were systematically compared with pathological results to succinctly summarize imaging features and elucidate their associations with both clinical and pathological characteristics.

Results All eight cases within this cohort exhibited abdominal-pelvic masses, comprising six solitary masses and two instances of multiple nodules, except for one case located in the left kidney, the remaining cases lacked a clear organ source. On plain images, seven cases exhibited patchy areas of low density within the masses, four cases showed calcification within the masses. Post-contrast imaging displayed mild-to-moderate, uneven enhancement. Larger masses displayed patchy areas without significant enhancement at the center. In the four MRI examinations, T1-weighted images exhibited uneven, low signal intensity, while T2-weighted images demonstrated uneven high signal intensity. Imaging unveiled four cases of liver metastasis, four cases of ascites, seven cases of lymph node metastasis, three cases of diffuse peritoneal thickening, and one case involving left ureter invasion with obstruction. In the FDG-PET/CT examinations of seven cases, multiple abnormal FDG accumulations were observed in the abdominal cavity, retroperitoneum, pelvis, and liver. One postoperative case revealed a new metastatic focus near the colonic hepatic region. The range of maximum standardized uptake values (SUV_{max}) for all lesions are 6.62–11.15.

†Kaiwei Xu, Yi Chen, Wenqi Shen and Fan Liu contributed equally to this work.

*Correspondence:
Jian Zhang
zhangjianxie20@outlook.com
Changjing Zuo
changjing.zuo@qq.com
Jianhua Wang
wangjianhua@nbu.edu.cn

Full list of author information is available at the end of the article

Conclusions DSRCT is commonly seen in young men, and the imaging results are mostly multiple lesions with no clear organ source. Other common findings include intratumoral calcification, liver metastasis, ascites, peritoneal metastasis, and retroperitoneal lymph node enlargement. The combined use of CT, MRI and FDG-PET/CT can improve the diagnostic accuracy and treatment evaluation of DSRCT. However, it is imperative to underscore that the definitive diagnosis remains contingent upon pathological examination.

Keywords Desmotplastic Small Round Cell Tumor, Computed tomography, Positron emission tomography, Magnetic resonance imaging

Introduction

Desmoplastic Small Round Cell Tumor (DSRCT) is a rare malignant tumor of the small round cell family of soft tissues. It was first reported by Gerard and Rosai in 1989. However, it wasn't until 1991 that DSRCT was officially recognized as a distinct clinical-pathological entity [1]. DSRCT was more commonly observed in young to middle-aged males, with a male-to-female ratio ranging from 4 to 5 to 1. The primary clinical manifestation involves the presence of isolated or multiple soft tissue masses in the abdominal-pelvic and retroperitoneal regions, devoid of clear organ origins. Clinical manifestations are often associated with abdominal masses [2, 3]. Patients are often diagnosed at an advanced stage of the disease upon initial evaluation, with peritoneal and organ metastases, such as liver and lungs, being common [4, 5]. Research has also indicated an association between DSRCT and the chromosomal translocation t(11;22) (p13; q12), resulting in the EWSR1:WT1 fusion gene [6, 7]. The incidence of DSRCT is extremely low, approximately 0.2 cases per million people [8]. There is a limited number of reports utilizing a comprehensive approach with computed tomography (CT), magnetic resonance imaging (MRI), and positron emission tomography (FDG-PET)/CT multimodal imaging for diagnosing this condition [9, 10]. Although the diagnosis rate of colorectal diseases can be improved by computer aided diagnosis system, the diagnostic accuracy of DSRCT is still not ideal [11, 12]. This study retrospectively analyzes CT, MRI, and PET/CT multimodal imaging features in eight cases of DSRCT, cross-referencing with pathological results and literature. The aim is to provide a comprehensive summary of the multimodal imaging characteristics of DSRCT, contributing to an enhanced understanding of this condition.

Materials and methods

Clinical information

We analyzed data from eight DSRCT patients who underwent surgery and received pathological confirmation at various medical institutions, including the First Affiliated Hospital of Xiamen University, the First Affiliated Hospital of Ningbo University, the Second Hospital of Ningbo, Li Huili Hospital of Ningbo Medical Center, and the Shanghai Panorama Medical Imaging Diagnosis Center, from November 2012 to April 2022. This retrospective study was approved by the institutional review board of the First Affiliated Hospital of Ningbo University, and met the requirements for a waiver of written informed consent.

All patients were male, with ages ranging from 13 to 65 years and an average age of 28.25 years. Among the eight patients, all underwent abdominal and pelvic contrast-enhanced CT scans, and four also received enhanced MRI. Six patients underwent FDG-PET/CT preoperative examination. The imaging examination of the 8 patients are summarized in Table 1.

Imaging examinations

The examinations were conducted using a 256-slice CT scanner (GE Revolution; Philips Healthcare Brillance iCT) and a 16-slice CT scanner (GE Optima CT540). The scan parameters were as follows: a reconstruction layer thickness of 5 mm, a field of view of 230 mm, a voltage of 120 kV, a current of 200–300 mA, and a matrix of 256×256. All six patients underwent both plain and contrast-enhanced CT scans. For contrast-enhanced CT, 100 ml of non-ionic iodinated contrast agent (iopromide; Ultravist; Schering) was intravenously injected at a rate of 2.5 mL/s. Enhanced abdominal and pelvic CT scans were performed at 30s and 60s, respectively, following contrast agent injection.

Patients underwent MRI examinations using a 1.5T MRI scanner (Siemens Symphony and Avanto) and a 3.0T MRI scanner (Siemens MAGNETOM Vida). The abdominal MRI protocol included unenhanced axial and coronal T1-weighted sequences, axial T2-weighted sequences, and contrast-enhanced axial and coronal T1-weighted sequences. The pelvic MRI protocol comprised unenhanced axial and coronal T1-weighted sequences, axial and sagittal T2-weighted sequences, and contrast-enhanced axial, sagittal, and coronal T1-weighted sequences. Sequence parameters were as follows: T1-weighted fast field echo (FFE) sequence (TR/TE, 174–291/4.6 ms, slice thickness 8.0 mm, field of view 380–520 mm, matrix scan 256×256), T2-weighted turbo spin-echo sequence (TR/TE, 1600–3500/90 ms, slice thickness 5.0 mm, field of view 300–380 mm, matrix scan 256×256). A gadolinium-based contrast agent (Gadolinium-DTPA; Magnevist; Schering) was intravenously injected at a dose of 0.1–0.2 mmol/kg before contrast-enhanced MRI scans.

Table 1 Frequency of patient imaging

Number	CT	MRI	^{18}F-FDG PET/CT
1	yes	no	no
2	yes	yes	postoperation
3	yes	yes	yes
4	yes	yes	yes
5	yes	no	yes
6	yes	no	yes
7	yes	yes	yes
8	yes	no	yes

Patients underwent examinations using PET/CT systems (Siemens Biograph m CT Flow 64; Siemens Biograph 64). Patients fasted for 6 h, and blood glucose levels were measured before ^{18}F-FDG injection to ensure glucose levels were <8.1 mmol/L. Insulin was administered subcutaneously if necessary. ^{18}F-FDG (4.4–7.4 MBq/kg) was intravenously injected, and patients lay in a dark room for 45–60 min before urinating prior to PET/CT imaging. Patients were positioned supine, and the scan was performed from the skull to the mid-thigh. A CT scan was conducted before PET, and the acquired data were used to generate attenuation correction maps for PET. PET images were reconstructed with a slice thickness of 3.75 mm using the ordered subset expectation maximization iterative reconstruction method. PET, CT, and fused PET/CT images were regenerated on a computer workstation for review.

Two experienced radiologists, blinded to the pathological diagnosis, analyzed the CT, MR, and FDG PET/CT imaging features of the lesions. This analysis included the location, shape, size, number, margins, and enhancement patterns of the lesions in both unenhanced and enhanced images. The radiological findings from CT, MRI, and FDG PET/CT were then compared with the pathological results. In cases of disagreement, consensus was reached through discussion.

Pathological analysis

Among the 8 patients, 2 underwent tumor resection followed by general observation, microscopic examination, and immunohistochemical testing. Additionally, the remaining 6 patients underwent needle biopsy, followed by microscopic examination and immunohistochemical testing. Immunohistochemical markers included CK (pan), desmin, CD99, vimentin, CAM5.2, EMA, Wilms Tumor, WT-1, and Ki-67.

Table 2 Frequency of abdominal imaging

Finding	No. of Patients（%）
Soft-tissue masses	8（100）
Central low attenuation	7（87.5）
Calcification	4（50）
Hepatic metastases	4（50）
Pulmonary metastasis	0（0）
Brain metastases	0（0）
Ascites	4（50）
Hydronephrosis	2（25）
Lymphadenopathy	7（87.5）
Diffuse peritoneal thickening	3（50）
Bowel obstruction	2（25）

Results

CT features

Abdominal Imaging Results are presented in Table 2. All eight patients exhibited masses in the abdominal-pelvic region, with one case demonstrating a mass in the left kidney, while the remaining cases showed masses without a clearly identifiable organ of origin. Among the masses with no clear organ of origin, five presented as solitary masses (three were located in the pelvic rectovesical space, one in the lesser omentum, and one large mass involved both the abdominal and pelvic cavities). Additionally, two cases presented with multiple masses in the abdominal-pelvic region. The maximum dimensions of the masses ranged from approximately 18 cm × 12 cm × 6 cm to a minimum of approximately 7 cm × 6 cm × 6 cm. On CT plain images, all eight cases appeared as soft tissue masses, with seven showing patchy areas of low density within the masses. Four cases exhibited calcification within the masses (Fig. 1a). Post-contrast imaging revealed mild-to-moderate, uneven enhancement of the masses, with larger masses displaying patchy areas without significant enhancement at the center (Fig. 1b). Notably, one large mass situated in the mid-lower abdominal wall peritoneal region exhibited unclear borders with adjacent intestinal segments, with multiple fluid-filled dilations observed in the ascending colon and portions of the small intestine (Fig. 1c and d).

MRI features

A total of four patients underwent contrast-enhanced MRI examinations. Lesions were visible on T1-weighted images as patchy, slightly low-signal areas, while on T2-weighted images, they exhibited uneven high-signal intensity. Contrast-enhanced T1-weighted images showed

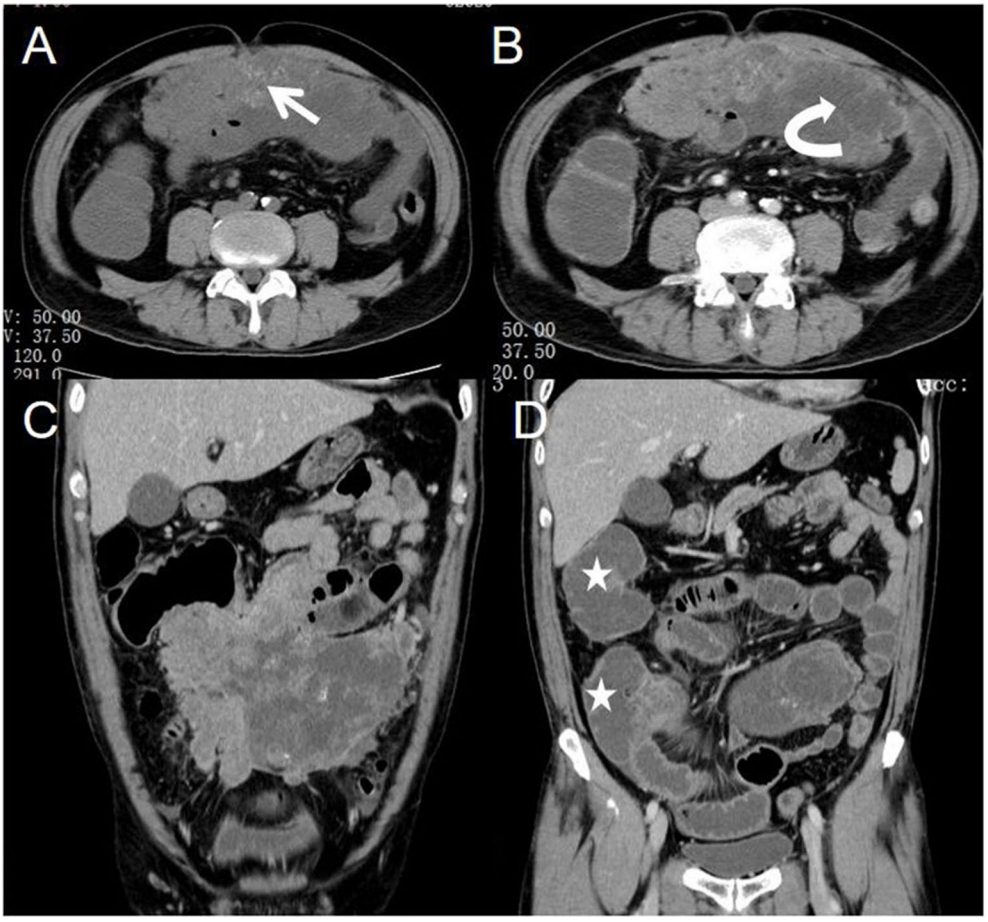

Fig. 1 A 65-year-old male patient presenting with abdominal mass sensation and incomplete intestinal obstruction. **A** The tumor is mainly located in the peritoneal area, with spotted calcification visible(arrow), and the boundary with the adjacent bowel duct is unclear; **B** In the arterial phase after contrast enhancement, the tumor shows mild-to-moderate, uneven enhancement, with patchy areas of low-enhancement visible within (curved arrow); **C** The tumor exhibits unclear borders with the surrounding intestinal segments; **D** Multiple fluid-filled dilations are observed in the ascending colon and portions of the small intestine (asterisk)

marked, uneven enhancement (Fig. 2a-d). Among these MRI patients, two exhibited liver metastasis, one presented with ascites, four showed lymph node metastasis, and one displayed diffuse peritoneal thickening (Fig. 2e).

FDG PET/CT features

Six patients underwent FDG-PET/CT examination. One patient exhibited a mass in the left kidney with abnormal FDG uptake, accompanied by metastasis to the left renal hilum, retroperitoneum, and para-aortic lymph nodes, as well as multiple bone metastases throughout the body (Fig. 3). Two patients presented with mixed density masses in the rectovesical space, showing abnormal FDG accumulation. Among them, one patient also had abnormal FDG concentration in the left upper abdomen, pelvic peritoneum, liver, and multiple lymph nodes throughout the body (Fig. 2e). One patient had multiple abnormal FDG accumulations in the lesser omentum and liver. The remaining two patients had multiple masses in the abdomen and pelvic region. Axial and corresponding fused FDG-PET/CT images revealed increased metabolism in the liver, abdomen, pelvis, and mediastinal lymph nodes. In one of these cases, mid-segmental hydronephrosis of the left ureter was observed, indicating tumor invasion with obstruction. The SUV_{max} range for all lesions was 6.62–11.15.

Pathologic findings

In the cohort of eight patients, two underwent surgical excision. The excised tumors were non-encapsulated, appearing gray-white on the cut surface, with visible areas of hemorrhage and necrosis in the center. Additionally, the remaining six patients underwent needle biopsy for pathological examination.

The pathological diagnosis of the tumors was consistent with DSRCT. The tumor cells exhibited a relatively loose arrangement, surrounded by desmoplastic proliferative stroma. The tumor cells were small, predominantly round or oval in shape, with sparse cytoplasm in most cells. The nuclei were deeply stained and appeared either round or oval.

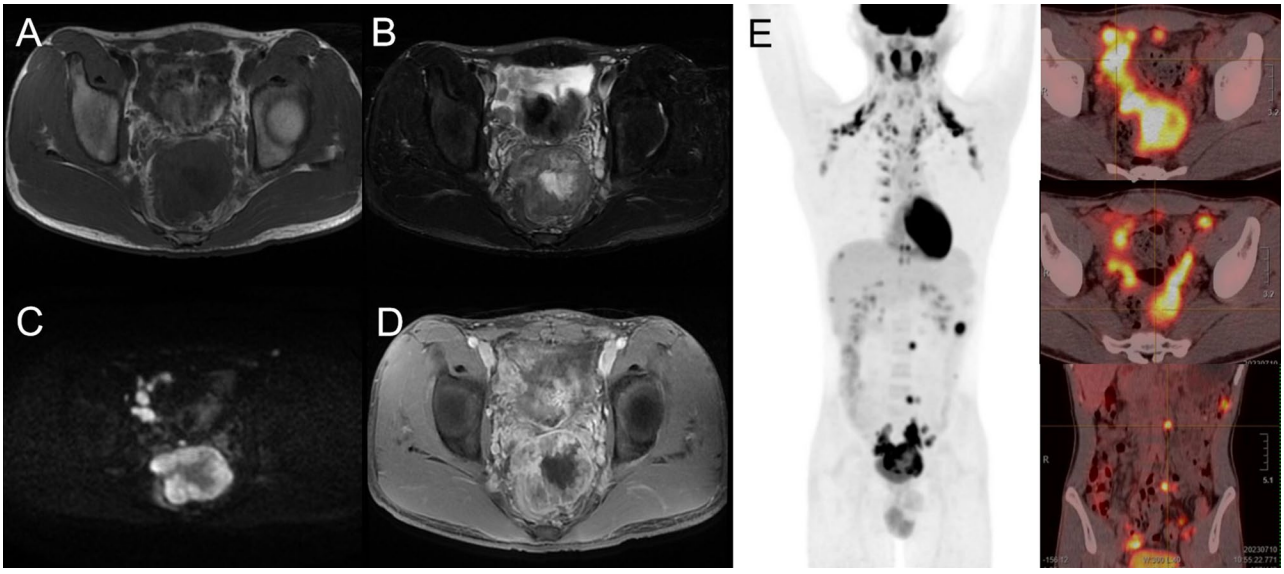

Fig. 2 A 20-year-old male presented with persistent lower abdominal pain and distension without apparent cause for one day. MRI images revealed irregular abnormal signal shadows in the rectovesical space. **A** Axial T1-weighted image showed slightly low signal intensity. **B** Axial T2-weighted image exhibited mixed high and low signal intensity. **C** Diffusion-weighted imaging presented mixed high signal intensity. **D** Contrast-enhanced axial T1-weighted image showed multiple prominent, uneven enhancements of the tumor. **E** FDG PET/CT images demonstrate increased metabolism in multiple regions, not only in the pelvic lesion area but also in the left upper abdomen, liver, and multiple pelvic and abdominal lymph nodes, with an SUV ranging from 3.42 to 11.15

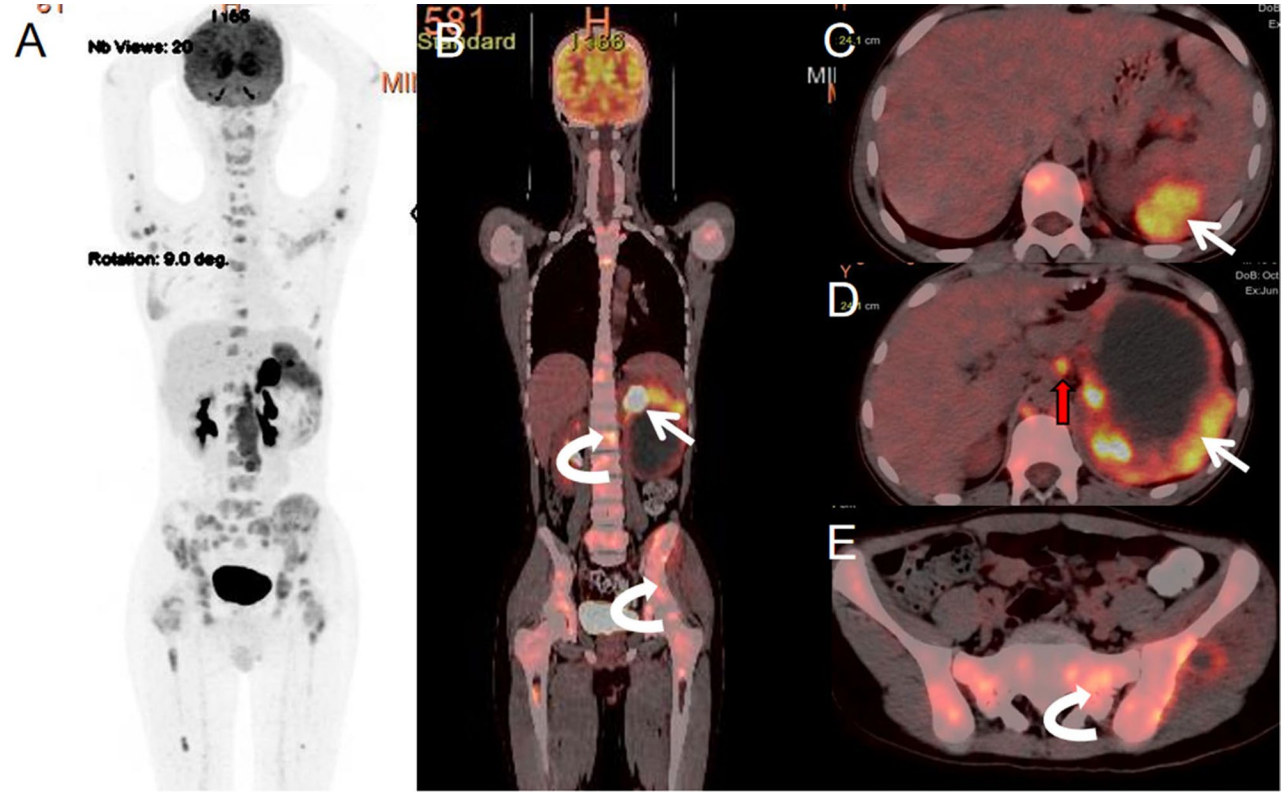

Fig. 3 A 13-year-old male presented with bilateral hip pain accompanied by intermittent fever for over two weeks. **A-E** FDG-PET/CT images revealed a cystic-solid mass with increased FDG uptake in the left renal area (arrows), multiple enlarged lymph nodes in the Left perirenal, retroperitoneum, and para-aortic region with increased FDG uptake (SUV_{max} 8.8), as well as multiple bone metastases throughout the body (SUV_{max} 4.6) (curved arrows). Retroperitoneal lymph node enlargement (red arrow)

The immunohistochemical results are as follows: In five cases, tumors showed positive expression for CK (pan), desmin, CD99, and vimentin. Among these, 2–4 cases demonstrated positive expression for CAM5.2, EMA, Wilms Tumor, and WT-1. Additionally, Ki-67 showed a positive expression ranging from 20 to 60% (Fig. 4).

Discussions

DSRCT was initially reported by Gerald and Rosai in 1989 [1]. It represents a rare malignant soft tissue tumor within the small round cell family. DSRCT primarily affects young to middle-aged males (male-to-female ratio 4–5:1) [2, 3]. Clinical presentations are often nonspecific, characterized by abdominal pain, distension, palpable abdominal masses, and may include constitutional symptoms such as weight loss and fatigue. Compression of surrounding organs may lead to manifestations like renal hydronephrosis and intestinal obstruction [2, 3, 13–16]. DSRCT commonly arises on the serosal surfaces within the peritoneal cavity and is frequently metastatic at the time of discovery. Involvement of the diaphragm and the retroperitoneum occurs in 40-50% of cases, and liver metastases are relatively common (>30%) [16]. Previous studies suggested a predilection for the pararectal spaces, with many cases presenting as multifocal pelvic masses. According to the imaging study conducted by Morani AC et al. on 94 patients with DSRCT, 90% of the patients presented with multiple abdominal and pelvic masses [16–19]. However, our study challenges this notion, as only three cases in our cohort were located in the rectovesical space, and two cases manifested as multifocal pelvic masses. Furthermore, within our cohort, there was one case localized to the left kidney. Since Su et al. [20] first reported primary renal DSRCT in 2004, a total of 13 cases have been documented in the literature [21, 22], consistent with previous reports [21], indicating a predilection for left renal involvement in renal DSRCT. The age range in our cohort of eight patients was 13–65 years, with a median age of 21 years. Notably, one patient presented at the age of 65, surpassing the typical range of 18–25 years [18]. Cases in this age group are rarely reported in the literature. Additionally, this patient exhibited a larger tumor measuring approximately 18 cm × 12 cm × 6 cm. Intraoperatively, we observed the tumor originating from the greater omentum, invading the midsection of the transverse colon, the anterior wall of the bladder, and the abdominal wall. No distant metastases were identified.

Routine imaging examinations such as CT and MRI play a crucial role in providing morphological information for patients with DSRCT, with CT being the preferred modality for diagnosis [23]. DSRCT typically manifests as solitary or multifocal lobulated soft tissue masses within the pelvic and abdominal peritoneum, lacking a defined organ of origin. Larger soft tissue masses may exhibit abnormal density changes such as necrosis, hemorrhage, or fibrous components [9]. In the study by Pickhardt et al., two out of nine patients presented with solitary masses, and seven had central low-density areas within the masses, with two showing calcifications [17]. In our research involving eight patients, six presented as solitary nodules, seven showed areas of low density within the lesions, and four exhibited calcifications.

Enhanced CT reveals mild-to-moderate enhancement in the masses, with larger masses potentially displaying peripheral enhancement [24, 25]. In comparison to CT, MRI offers unique advantages in delineating the extent of lesions and peritoneal metastasis [26]. DSRCT typically appears as heterogeneous low signal intensity on T1-weighted images and heterogeneous high signal intensity on T2-weighted images. Multisequence signal changes in MRI contribute to characterizing the components of DSRCT [27, 28]. In our case series, seven cases exhibited central low density/signal and non-enhancing areas on CT/MRI images, possibly indicative of central hemorrhagic necrosis within the tumor [9]. However, distinct features such as T1-weighted high signal and fluid-fluid levels suggesting hemorrhagic changes were not observed in this cohort. Notably, two cases in our series presented with cystic lesions near the stomach and in the left kidney, respectively, predominantly cystic in nature, with the cystic component located away from the central tumor area. Post-contrast imaging demonstrated mild-to-moderate

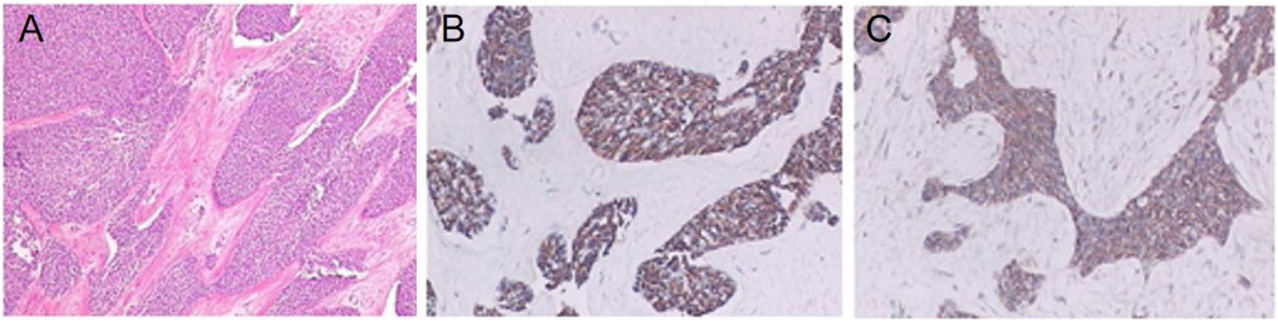

Fig. 4 Pathological images of a 39-year-old male. **A** Tumor cells arranged in a nest-like pattern, small and relatively uniform in size, with visible mitotic figures, indicating invasive growth of the tumor. **B** Immunohistochemical examination showing positive expression for desmin. **C** Immunohistochemical staining demonstrating positive expression for CD99

enhancement in the solid portion, while the cystic component showed no significant enhancement. This presentation, predominantly cystic and away from the central tumor area, is infrequently reported in previous cases.

FDG-PET/CT holds a functional imaging advantage, revealing metabolically active masses within the pelvic and abdominal peritoneum. Rosoff et al. noted changes in SUV values post-treatment in DSRCT, indicating that FDG-PET/CT can provide unique metabolic status information beyond what CT and MRI can measure. This is particularly advantageous in assessing treatment efficacy and detecting concealed lesions [18, 28, 29]. In our study, PET/CT examinations were conducted for a total of seven patients. Liver metastasis was identified in four case, multiple lymph node metastases in the pelvic and abdominal peritoneum were observed in seven cases, and one patient, during a follow-up three months post-surgery, exhibited metastatic lesions adjacent to the hepatic flexure of the colon. It is worth noting that in our cohort, there was one case with a lesion localized to the left kidney, which showed FDG-PET/CT findings of metastasis to the left renal hilum, retroperitoneal area, and para-aortic lymph nodes, as well as multiple bone metastases throughout the body. Previous reports on PET/CT findings in DSRCT involving the left kidney are scarce. These findings suggest that PET/CT, on the basis of CT and MRI, can aid in identifying the extent of DSRCT lesions, assessing systemic metastasis, and evaluating the effectiveness of tumor therapy.

In histopathology, tumor cells are surrounded by a proliferative connective tissue stroma, exhibiting a nested arrangement. The tumor cells are small in size, predominantly round or oval, with most cells having sparse cytoplasm and deeply stained nuclei. Immunohistochemically, tumor cells demonstrate multidirectional differentiation expressing various immune phenotypes, including EMA, keratin, NSE, vimentin, and desmin, among other markers [24, 30, 21]. This broad antigen expression profile is a characteristic feature of DSRCT and can be utilized to differentiate DSRCT from other tissue-related small round cell tumors [31]. Reported expression rates for the epithelial marker CAM5.2 and EMA are approximately 70% and 90%, respectively. Desmin is expressed positively in up to 72% of lesions, and its characteristic feature in DSRCT includes focal or diffuse distribution of subnuclear dots, consistent with previous literature [32, 33]. Our study results are in general agreement with the aforementioned literature. Additionally, while nearly all DSRCT cases in previous reports have shown positive expression for WT1, only two cases in our study exhibited WT1 positivity. This discrepancy may be attributed to variations in transcript variants altering the immunostaining pattern, suggesting the need to supplement both N-terminal and C-terminal regions as a form of "molecular immunohistochemistry" for identifying EWS-WT1 transcripts [31].

The differential diagnosis of DSRCT includes rhabdomyosarcoma, malignant mesothelioma, primitive neuroectodermal tumors (PNETs), lymphoma, intra-abdominal desmoid fibromatosis, and neuroblastoma. DSRCT typically occurs in adolescents, especially males, presenting as isolated or multiple soft tissue masses without a clear organ of origin, which is a characteristic feature [17, 19]. Rhabdomyosarcoma occurs in 70% of cases in children under 10 years, with about 10% involving the peritoneum. Compared to DSRCT, rhabdomyosarcomas typically have smaller tumors and almost no calcifications [34]. Malignant mesothelioma is rare in patients under 20 years, often accompanied by pleuroperitoneal effusion, possibly related to asbestos exposure [35]. Peritoneal leiomyosarcoma is more common in females over 24 years, and PNETs are highly invasive tumors that predominantly affect young individuals. Unlike DSRCT, PNETs exhibit fewer calcifications. Lymphoma is common in middle-aged males and is characterized by thickening of the intestinal wall, enlargement of organs such as the liver and spleen, and lymph node enlargement. Additionally, calcifications and peritoneal nodules are less common in lymphomas. Intra-abdominal desmoid tumor is a rare benign fibrous tissue proliferation that predominantly occurs in females. It can occur as an isolated entity or be associated with Gardner syndrome. Compared to DSRCT, desmoid fibromatosis rarely undergoes necrosis or cystic changes and does not metastasize. Neuroblastoma is another differential diagnosis, with onset typically before the age of 5, usually presenting as a single paravertebral mass, making it easier to differentiate from DSRCT [9, 16, 24].

Due to limitations in sample size and study design, this research is inevitably subject to certain biases. To address the sampling bias associated with the small sample size, we implemented the following strategies: (1) Cases were collected from multiple provinces across China, ensuring a relatively broad and representative sample. Multicenter data collection is an effective strategy to minimize sampling bias. (2) These eight cases represent all pathologically confirmed DSRCT diagnoses from five institutions between November 2012 and April 2022, with no selective criteria that could introduce bias. Despite the limited sample size, this study remains valuable for research on rare diseases. Furthermore, to mitigate potential observer bias, we adopted the following measures: (1) Both radiologists were highly experienced, blinded to clinical data, and conducted independent evaluations before reaching a consensus, thereby reducing the risk of observer bias during the initial assessment phase. (2) Both radiologists adhered to a standardized imaging protocol to ensure consistency. We acknowledge that discussing the potential impact of observer bias enhances the transparency and rigor of our methodology. With these measures in place, we believe the results of this study are both reliable and applicable (Table 3).

Table 3 Imaging findings of DSRCT patients

References	Cases	imaging examination	Age	Sex(men: women)	location	Central low attenuation	Calcification	peritoneal metastasis	Hepatic metastases
Chen J et al. [9]	4	CT: 4; FDG-PET/CT: 1	14–31	4:0	Multiple large masses in the abdominopelvis: 4 cases	4/4	2/4	3/4	3/4
Zhang WD et al. [10]	7	CT: 5; MRI: 2; FDG-PET/CT: 2	22–31	7:0	Multiple large masses in the abdominopelvis: 6 cases; a mass in the pelvis: 1 case	5/7	3/7	3/7	2/7
Morani AC et al. [16]	94	unknown	5–53	43:4	multifocal masses, nodular masses, diffuse omental and peritoneal masses:85 cases (90%)	unknown	12/94	49/94	32/94
Pickhardt PJ et al. [17]	9	CT: 9; US:3	4–36	5:4	predominantly intraperitoneal	7/9	2/9	1/9	3/9
Thomas R et al. [18]	20	CT: 20; MRI: 5	15–46	4:1	multiple peritoneal/omental soft tissue masses: 17 cases; solitary peritoneal mass: 2 cases	10/20	4/20	19/20	4/20
Bellah R et al. [19]	11	CT: 11	10–20	8:3	multiple omental, serosal, or mesenteric masses: 11 cases	unknown	6/11	6/11	6/11
Li G et al. [23]	12	CT: 12	14–39	2:1	intraperitoneal: 7 cases; omentum and/or paravesical and pararectal region: 5 cases	4/11	2/11	9/11	2/11
Tateishi U et al. [25]	4	CT: 4; MRI: 4	18–32	4:0	situated within omentum and paracolic gutter: 4 cases	3/4	4/4	2/4	3/4
Ostermeier A et al. [29]	8	FDG-PET/CT: 8	2–20	7:1	widespread disease: 6 cases; localized disease: 2 cases	unknown	unknown	unknown	1/8
our research	6	CT: 6; MRI: 3; FDG-PET/CT: 4	17–65	6:0	abdominal pelvic omentum (multiple): 2 cases; rectovesical space: 2 cases; abdominal pelvic omentum: 1 case; lesser omentum: 1 case.	5/6	2/6	3/6	1/6

Conclusions

This set of cases highlights the diagnostic challenges associated with DSRCT and underscores the critical role of multimodal imaging modalities (CT, MRI, and PET/CT) in delineating DSRCT lesion extent, assessing for systemic metastasis, and evaluating treatment efficacy. Nonetheless, histopathology and immunohistochemistry remain the definitive gold standards for diagnosis. Compared to prior studies, this study provides several distinctive advantages: (1) Two cases in this study presented as cystic-solid masses located near the stomach and left kidney, with cystic alterations found in non-central areas of the lesions, a rare finding in previous reports; (2) This study draws from multiple centers, offering comprehensive multimodal imaging data, including CT, MRI, and PET/CT. Notably, a case of left renal DSRCT—a particularly rare presentation—is included; only 13 such cases have been documented in the literature, with minimal specific PET/CT findings reported for left renal DSRCT. This case series addresses a significant gap in the PET/CT research related to renal DSRCT, providing a valuable addition to the existing literature on DSRCT.

Acknowledgements
None.

Author contributions
KX, YC and WS are the primary authors of the manuscript. JW, CZ, JZ are the supervising and corresponding author. All remaining authors contributed equally to the paper and read and approved the final manuscript.

Funding
This research is funded by Funds of the National key research and development program (No. 2022YFC2010001), the National Natural Science Foundation of China (No. 82172004), the project of medicine and health of zhejiang province (No. 2024KY315), the Ningbo Natural Science Foundation (No. 2021J254), Ningbo Clinical Research Center for Medical Imaging (No.2022LYKFYB04) and the project of Ningbo leading Medical&Health Discipline (No. 2022-B15).

Data availability
No datasets were generated or analysed during the current study.

Declarations

Ethics approval and consent to participate
The study design was approved by the appropriate ethics review board.

Consent for publication
Not applicable.

Competing interests
The authors declare no competing interests.

Author details
[1]Health Science Center, Ningbo University, 818 Fenghua Road, Ningbo 315211, People's Republic of China
[2]Department of Radiology, Ningbo Medical Center of Lihuili Hospital of Ningbo University, 57 Xingning Road, Ningbo 315040, People's Republic of China
[3]Department of Radiology, The First Affiliated Hospital of Ningbo University, 59 Liuting Street, Ningbo 315010, People's Republic of China
[4]Department of Radiology, The First Affiliated Hospital of Xiamen University, 55 Zhenhai Road, Xiamen 361000, People's Republic of China
[5]Shanghai Universal Medical Imaging Diagnostic Center, Building 8, 406 Guilin Road, Xuhui District, Shanghai 201103, People's Republic of China
[6]Department of Nuclear Medicine, Changhai Hospital, Naval Medical University, 168 Changhai Road, Shanghai 200433, People's Republic of China

Received: 20 August 2024 / Accepted: 18 November 2024
Published online: 18 December 2024

References

1. Domanski HA. The small round cell sarcomas complexities and desmoplastic presentation. Acta Cytol. 2022;66(4):279–94.
2. Gerald WL, Miller HK, Battifora H, et al. Intra-abdominal desmoplastic small round-cell tumor. Report of 19 cases of a distinctive type of high-grade polyphenotypic malignancy affecting young individuals. Am J Surg Pathol. 1991;15(6):499–513.
3. Roberts P, Burchill SA, Beddow RA, et al. A combined cytogenetic and molecular approach to diagnosis in a case of desmoplastic small round cell tumor with a complex translocation (11;22;21). Cancer Genet Cytogenet. 1999;108:19–25.
4. Honoré C, Amroun K, Vilcot L, et al. Abdominal desmoplastic small round cell tumor: multimodal treatment combining chemotherapy, surgery, and radiotherapy is the best option. Ann Surg Oncol. 2015;22(4):1073–9.
5. Hendricks A, Boerner K, Germer CT, et al. Desmoplastic small round cell tumors: a review with focus on clinical management and therapeutic options. Cancer Treat Rev. 2021;93:102140.
6. Philippe-Chomette P, Kabbara N, Andre N, et al. Desmoplastic small round cell tumors with EWS-WT1 fusion transcript in children and young adults. Pediatr Blood Cancer. 2012;58(6):891–7.
7. Xiang T, Zhang SY, Wang SS, et al. A nationwide analysis of desmoplastic small round cell tumor. Med (Baltim). 2020;99(30):e21337.
8. Stacchiotti S, Frezza AM, Blay JY, et al. Ultra-rare sarcomas: a consensus paper from the Connective Tissue Oncology Society community of experts on the incidence threshold and the list of entities. Cancer. 2021;127(16):2934–42.
9. Chen J, Wu Z, Sun B, et al. Intra-abdominal desmoplastic small round cell tumors: CT and FDG-PET/CT findings with histopathological association. Oncol Lett. 2016;11(5):3298–302.
10. Zhang WD, Li CX, Liu QY, et al. CT, MRI, and FDG-PET/CT imaging findings of abdominopelvic desmoplastic small round cell tumors: correlation with histopathologic findings. Eur J Radiol. 2011;80:269–73.
11. Bakkouri I, Bakkouri S. 2MGAS-Net: multi-level multi-scale gated attentional squeezed network for polyp segmentation. SIViP. 2024;18:5377–86.
12. Bakkouri I, Afdel K, DermoNet. A computer-aided diagnosis system for dermoscopic disease recognition. Lect Notes Comput Sci. 2020;12119:170–7.
13. Vujić G, Mikuš M, Matak L, et al. Desmoplastic Small Round Cell Tumor of the Ovary: a Case Report with a new modality of treatment and review of the literature. Rev Bras Ginecol Obstet. 2020;42(5):297–302.
14. Atef A, Gaballa K, Zuhdy M, et al. Primary desmoplastic small-round-cell tumor of the ovary. J Egypt Natl Canc Inst. 2019;31(1):4.
15. Lee HJ, Hyun JS, Jang HS, et al. Paraneoplastic secondary hypertension due to a renin-secreting desmoplastic small round cell tumor: a case report. Oncol Lett. 2014;8(5):1986–92.
16. Morani AC, Bathala TK, Surabhi VR, et al. Desmoplastic Small Round Cell Tumor: imaging pattern of Disease at Presentation. AJR Am J Roentgenol. 2019;212(3):W45–54.
17. Pickhardt PJ, Fisher AJ, Balfe DM, et al. Desmoplastic small round cell tumor of the abdomen: radiologic-histopathologic correlation. Radiology. 1999;210(3):633–8.
18. Thomas R, Rajeswaran G, Thway K, et al. Desmoplastic small round cell tumour: the radiological, pathological and clinical features. Insights Imaging. 2013;4(1):111–8.
19. Bellah R, Suzuki-Bordalo L, Brecher E, et al. Desmoplastic small round cell tumor in the abdomen and pelvis: report of CT findings in 11 affected children and young adults. AJR Am J Roentgenol. 2005;184(6):1910–4.
20. Su MC, Jeng YM, Chu YC. Desmoplastic small round cell tumor of the kidney. Am J Surg Pathol. 2004;28:1379–83.
21. Ertoy Baydar D, Armutlu A, Aydin O, et al. Desmoplastic small round cell tumor of the kidney: a case report. Diagn Pathol. 2020;15(1):95.

22. Liu Y, Tao Y, Wang F, et al. Desmoplastic Small Round Cell Tumor of the kidney with mainly pulmonary symptoms by F-FDG PET/CT. Urology. 2021;154:e15–6.
23. Li G, Wang HT, Gao Y, et al. Primary abdominopelvic desmoplastic small round cell tumor: CT and correlated clinicopathologic features. Eur Rev Med Pharmacol Sci. 2014;18(18):2670–7.
24. Chen W, Chen H, Zhao C, et al. Desmoplastic small round cell tumor: the report of two cases and literature analysis review of the radiological findings. Quant Imaging Med Surg. 2023;13(7):4762–9.
25. Tateishi U, Hasegawa T, Kusumoto M, et al. Desmoplastic small round cell tumor: imaging findings associated with clinicopathologic features. J Comput Assist Tomogr. 2002;26(4):579–83.
26. Campos NMF, Almeida V, Curvo Semedo L. Peritoneal disease: key imaging findings that help in the differential diagnosis. Br J Radiol. 2022;95(1130):20210346.
27. Kis B, O'Regan KN, Agoston A, et al. Imaging of desmoplastic small round cell tumour in adults. Br J Radiol. 2012;85(1010):187–92.
28. Rosoff PM, Bayliff S. Successful clinical response to irinotecan in desmoplastic round blue cell tumor. Med Pediatr Oncol. 1999;33(5):500–3.
29. Ostermeier A, McCarville MB, Navid F, et al. FDG PET/CT imaging of desmoplastic small round cell tumor: findings at staging, during treatment and at follow-up. Pediatr Radiol. 2015;45(9):1308–15.
30. Gorospe L, Gómez T, González LM, et al. Desmoplastic small round cell tumor of the pelvis: MRI findings with histopathologic correlation. Eur Radiol. 2007;17(1):287–8.
31. Zhou J, Li Q, Luo B, et al. Primary desmoplastic small round cell tumor of the submandibular gland: a case report and literature review. Diagn Pathol. 2022;17(1):6.
32. Thway K, Noujaim J, Zaidi S, et al. Desmoplastic Small Round Cell Tumor: Pathology, Genetics, and potential therapeutic strategies. Int J Surg Pathol. 2016;24(8):672–84.
33. Matute G, Franco Mira JA, Arroyave Toro A, et al. A Classic Presentation of Desmoplastic Small Round Cell Tumor. Cureus. 2021;13(8):e17582.
34. Chung CJ, Bui V, Fordham LA, et al. Malignant intraperitoneal neoplasms of childhood. Pediatr Radiol. 1998;28(5):317–21.
35. Haliloglu M, Hoffer FA, Fletcher BD. Malignant peritoneal mesothelioma in two pediatric patients: MR imaging findings. Pediatr Radiol. 2000;30(4):251–5.

Publisher's note